Electronic Supplementary Material (ESI) for Chemical Communications.

Supplementary Information: Enhanced Hydrogen Bonding via Epoxide-functionalization Restricts Mobility in Poly(ethylenimine) for CO_2 Capture

Sichi Li,[*,†] Marcos F. C. Andrade,[†] Anthony J. Varni,[†] Glory A. Russell-Parks,[‡,¶]
Wade A. Braunecker,[‡,¶] Elwin Hunter-Sellars,[†] Maxwell A. T. Marple,[†] and
Simon H. Pang[*,†]

†*Materials Science Division, Lawrence Livermore National Laboratory, Livermore, CA 94550, USA*

‡*National Renewable Energy Laboratory, 15013 Denver West Parkway, Golden, Co 80401, USA*

¶*Department of Chemistry, Colorado School of Mines, 1500 Illinois St., Golden, CO 80401, USA*

E-mail: li77@llnl.gov; pang6@llnl.gov

Contents

1 Computational details

1.1 Constrained ab initio molecular dynamics and blue-moon ensemble

Free energy profiles of H bonding were computed using the blue-moon ensemble method, by integrating constraint forces sampled over constrained ab initio molecular dynamics (AIMD) simulations along predefined reaction coordinates. Constrained AIMD simulations were performed with the Vienna ab initio simulation package (VASP), version 5.4.4,[1] using the projector augmented wave treatment of core-valence interactions[2,3] with the Perdew-Burke-Ernzerhof (PBE) generalized gradient approximation[4] for the exchange-correlation energy. DFT-D3 method of Grimme et al. was employed for vdW-dispersion energy corrections.[5] Different combinations of amine or hydroxyl-containing small molecules, shown in Figure S1, were used in all simulations as molecular proxies to approximate H bond acceptors and donors in PEI. A 15 Å × 15 Å × 15 Å cubic supercell was used to accommodate each acceptor/donor pair. The Brillouin zone was sampled at the Γ-point only with a energy cutoff of 400 eV. All hydrogen atoms were substituted by deuterium to allow a time step of 1ps. For each time step, the electronic energy was converged to 10^{-4} eV. 10 ps of NVT AIMD simulations at 298 K using a Nos$\acute{e}$-Hoover thermostat[6] were run to pre-equilibrate structures before initiating constrained AIMD. The acceptor-donor distances are fixed in each simulation and the constraint forces were averaged over the final 8 ps of the 10ps trajectories to obtain the free energy profiles. Free energy profiles are shown as smooth curves based on cubic spline data interpolation of discrete data points, exampled in Figure S2. To assess the accuracy of PBE+D3 for capturing H bond interactions, we performed Constrained AIMD simulations but with SCAN functional[7] for two H bonds, one involving only amines and the other involving a amine-hydroxyl pair. As shown in Figure S3, the discrepancy between bond formation energies predicted by PBE+D3 and SCAN is small. In specific, SCAN consistently predicts slightly lower bond formation energies compared to PBE+D3, by only ≈ 2 kJ/mol, suggesting that the free energy profiles determined by PBE+D3 are reliable, especially when being used for comparison across different H bonds.

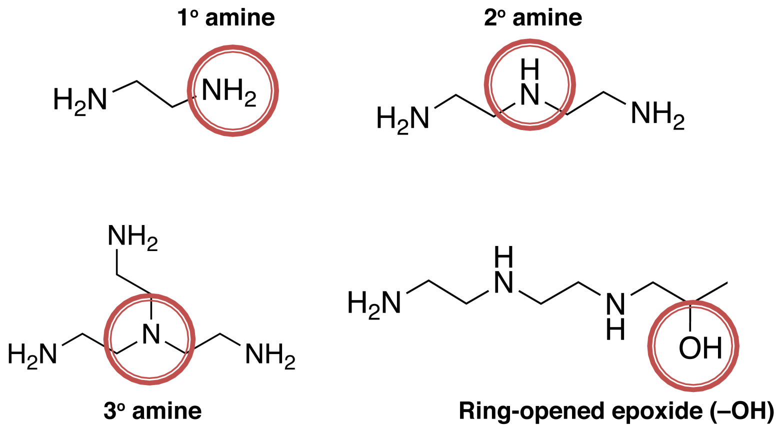

Figure S1: Molecular proxies for potential H bond donors and acceptors in PEI.

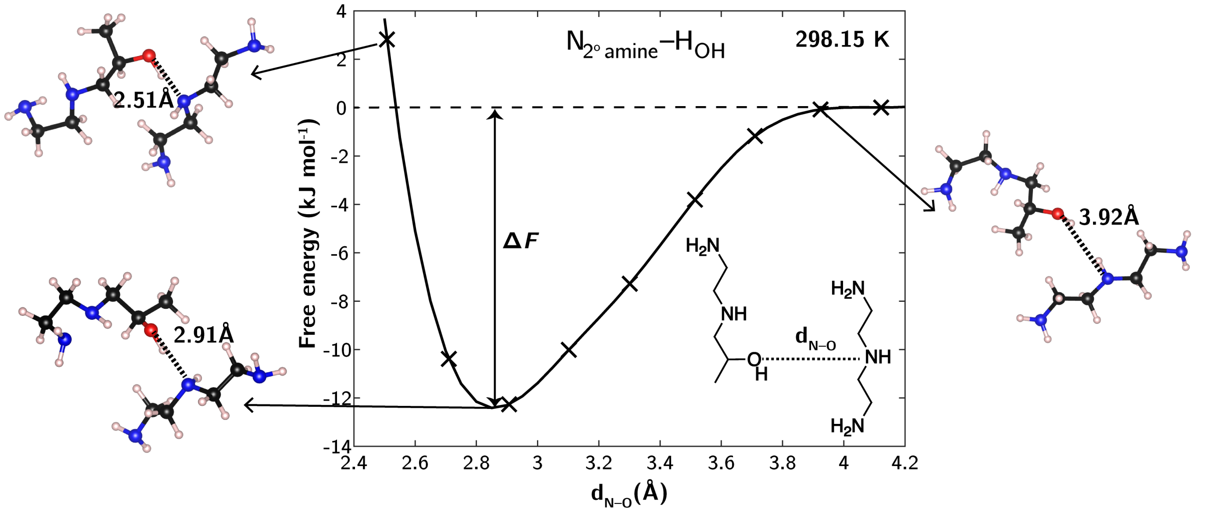

Figure S2: Free energy profile of H bond between a hydroxyl group and a 2° amine constructed from constrained AIMD simulations. Each discrete data point, shown as black cross, corresponds to one constrained AIMD simulation with specific fixed acceptor-to donor distance, in this case $d_{\text{N-O}}$. To better illustrate the specified reaction coordinate, snapshots of molecular structures are shown for three $d_{\text{N-O}}$. The bond free energy (ΔF) is defined as the energy of the local minimum relative to the flat region at large $d_{\text{N-O}}$. Color code: black - C, blue - N, red - O, pink - H.

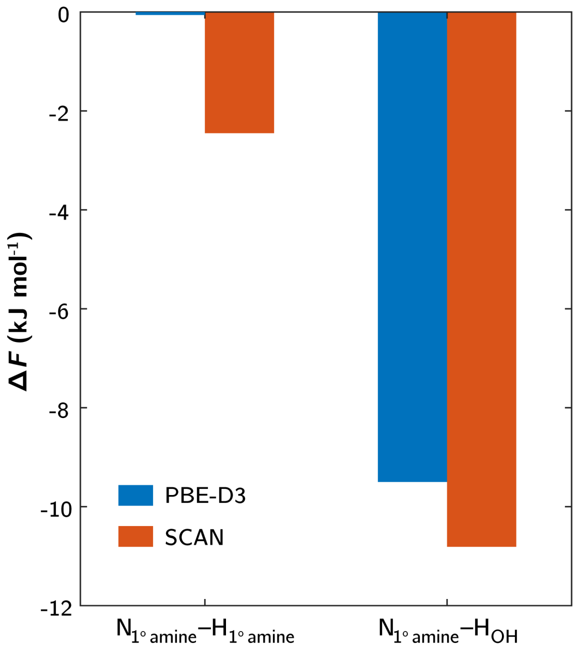

Figure S3: Comparison of ΔF computed using PBE+D3 vs. SCAN for two different H bonds.

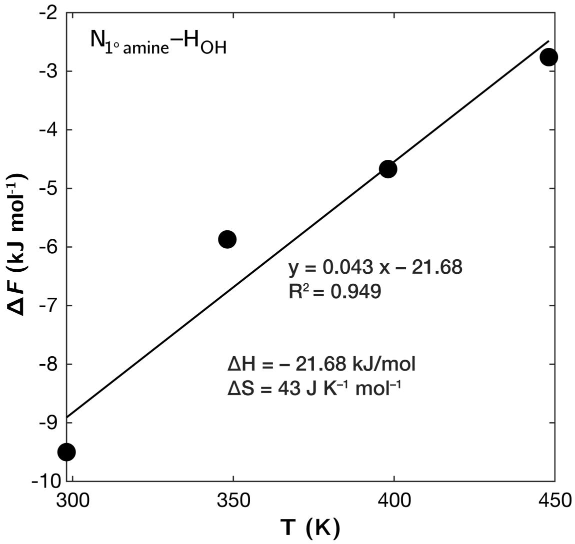

Figure S4: ΔF as a function temperature for $\mathrm{N}_{1^{\circ}\ \mathrm{amine}}$—$\mathrm{H}_{\mathrm{OH}}$. Linear regression was performed to determine the underlying ΔH and ΔS.

1.2 Deep potential molecular dynamics

NPT molecular dynamics simulations of PO-functionalized TETA dissolved in liquid TETA were performed with a deep neural network (DNN) potential trained on the density functional SCAN.[7] The construction of the DNN potential followed the smooth version of the Deep Potential Molecular Dynamics method,[8] using a 3-layers deep neural network with 60 neurons per layer. The input descriptor for the DNN consisted of the chemical environment within 6 Å radius of each atom, smoothly decaying from 1 Å. The training data of the DNN were collected through the active learning method proposed by Zhang et al.,[9] and it included configurations of liquid TETA and PO-functionalized TETA dissolved in liquid TETA explored at 300 K and 1 bar. Calculations using the density functional SCAN employed Troullier Martins pseudopotentials,[10] with wavefunctions and electron density planewave-expanded at 200 and 800 Ry cutoff, respectively. Molecular dynamics were performed on periodically repeating systems containing 72 TETA or 64 TETA and 8 PO-functionalized TETA molecules per unit cell. Temperature was controlled at 300 K and pressure kept at 1 bar using a Nosé-Hoover thermostat chain[6] with 3 beads and the Parrinello-Rahman barostat,[11] respectively.

The DNN was trained using the DeepMD-kit code[12] (version 2.1.5), and all molecular dynamics simulations were carried out with the Lammps code[13] interfaced with DeepMD-kit. First principles calculations using the SCAN functional were performed with the PWscf code of Quantum-ESPRESSO[14] package (version 6.8) interfaced with Libxc (version 4.3.4).

The dynamic stability of the H bond network, i.e. H bond survival probability, is studied through a history-dependent time correlation function of H-bonds.[15] This function, P(t), measures the probability that a H-bond between atoms types *i* and *j* will be intact over an entire period *t*. The expression of $\mathrm{P}_{ij}(\mathrm{t})$ is given below

$$P_{ij}(t) = \frac{\langle h_{ij}(t)h_{ij}(0)\delta(\int_0^\tau [1 - h_{ij}(t)]d\tau)\rangle}{\langle h_{ij}\rangle} \tag{1}$$

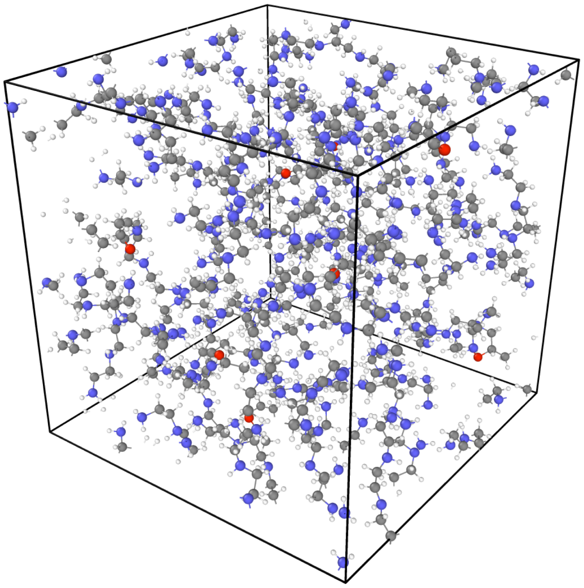

Figure S5: A snapshot of the simulation cell employed for the DPMD simulation of partially PO-functionalized liquid TETA. Atom colors: C-gray, N-blue, O-red, H-pearl white.

with $\mathrm{h}_{ij}(\mathrm{t})$ equals to 1 if a pair of atoms with types i and j are H-bonded and zero otherwise. The definition of an intact $\mathrm{H_2O{-}H_2O}$ H bond adopted is (i) $\mathrm{d_{O\text{-}O}} < 3.5$ Å and (ii) $\theta_{\mathrm{O\text{--}H\text{-}O}} < 30°$ as suggested by Starr et al.[16] A similar definition is adopted for an intact amine-hydroxyl H bond as its equilibrium acceptor-to-donor distance (Figure 1) is similar to that of a water-water H bond:[17] $\mathrm{d_{N\text{-}O}} < 3.5$ Å and $\theta_{\mathrm{N\text{--}H\text{-}O}} < 30°$. Figure 1 shows that the equilibrium acceptor-to-donor distance of an amine-amine H bond is roughly 0.5 Å longer than an amine-hydroxyl H bond, so a looser distance definition is used while the angle definition remains the same: $\mathrm{d_{N\text{-}N}} < 4$ Å and $\theta_{\mathrm{N\text{--}H\text{-}N}} < 30°$. The brackets in this expression indicate average over initial time and over pairs of atoms $i - j$ initially H-bonded at t=0. The delta function is defined as $\delta(x) = 1$ if $x = 0$, and $\delta(x) = 0$ if $x \neq 0$.

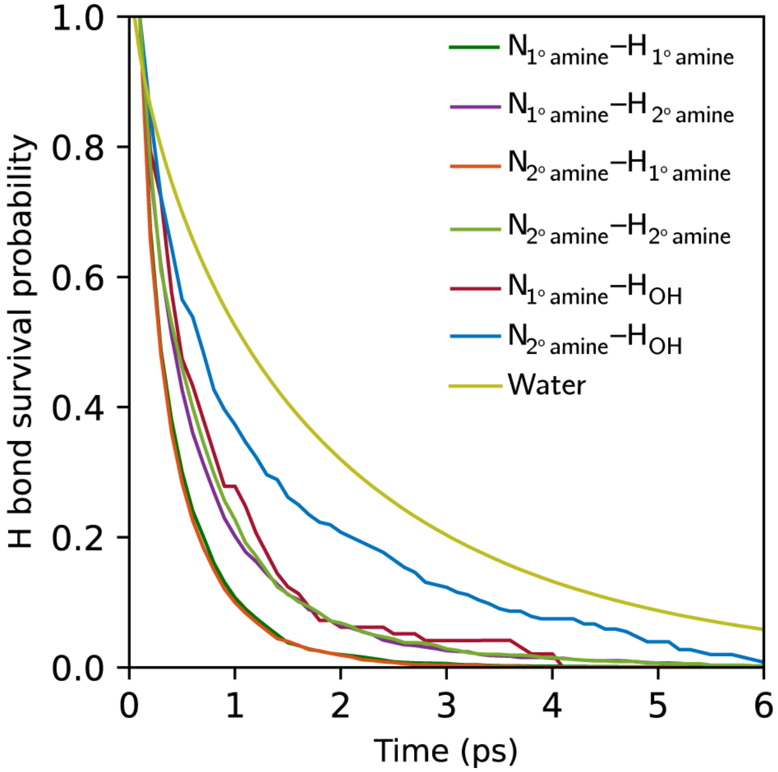

Figure S6: H bond survival probability averaged over all hydrogen bonds of the same type from the DPMD trajectories of partially functionalized liquid TETA, and liquid water at 300 K and 1 bar.

2 Experimental details

2.1 Synthesis of PO-functionalized BPEI

2.1.1 0.2 O:N PO−BPEI

A 100 mL Schlenk flask was charged with branched poly(ethylenimine) (5.08 g, 118 mmol, Mw = 800 g/mol) and vacuum backfilled 3 times (with argon). 30 mL of anhydrous methanol was added, and after stirring for 10 minutes, propylene oxide (1.68 mL, 24.0 mmol) was added dropwise. The reaction mixture was stirred for 24 h at 22 °C. The methanol was then removed under high vacuum for 48 h at 22 °C and then 5 h at 50 °C, yielding a viscous, colorless liquid.

^{1}H NMR (500 MHz, D_2O) δ 3.86 (hept, J = 6.1 Hz, 1H), 2.95 – 2.29 (m, 21H), 1.11 (m, 3H). ^{13}C NMR (126 MHz, D_2O) δ 66.2, 65.7, 65.5, 65.3, 64.9, 61.7, 61.6, 56.3, 56.2, 55.7, 55.6, 53.7, 53.1, 51.0, 50.8, 50.7, 48.8, 47.7, 45.6, 39.9, 39.9, 37.8, 20.3, 19.7.

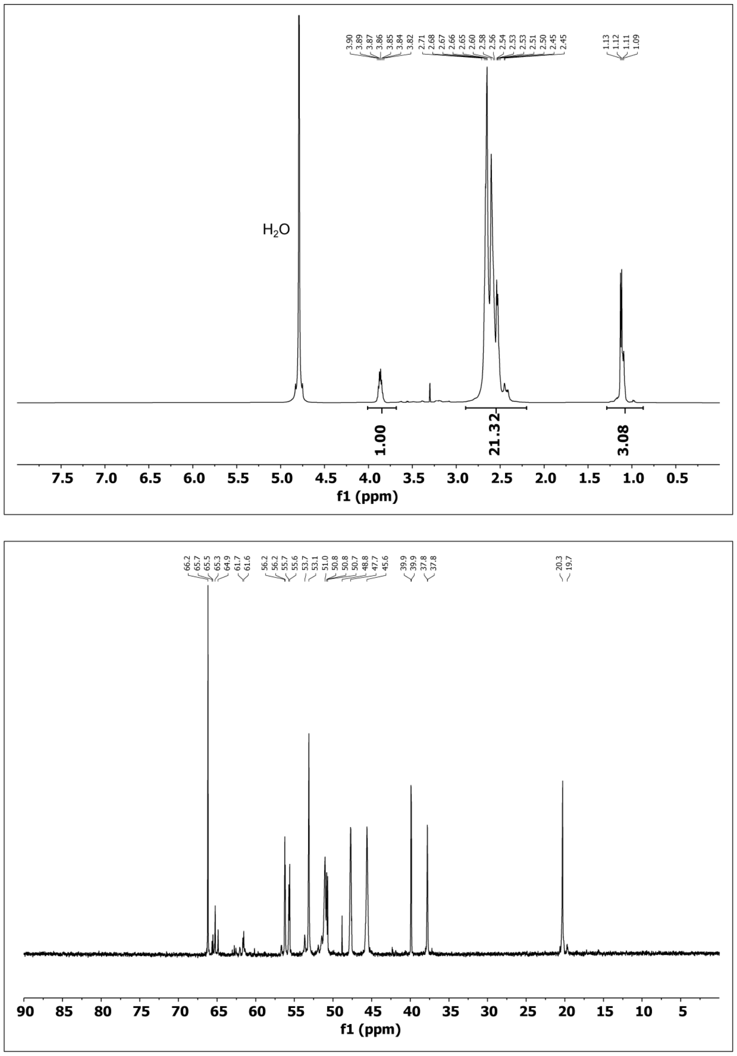

Figure S7: ^{1}H NMR spectrum (Top, 500 MHz) and ^{13}C NMR spectrum (Bottom, 126 MHz) of 0.2 O:N PO−BPEI collected in D_2O.

2.1.2 0.4 O:N PO−BPEI

A 100 mL Schlenk flask was charged with branched poly(ethylenimine) (5.06 g, 118 mmol, Mw = 800 g/mol) and vacuum backfilled 3 times (with argon). 30 mL of anhydrous methanol was added, and after stirring for 10 minutes, propylene oxide (3.36 mL, 48.0 mmol) was added dropwise. The reaction mixture was stirred for 24 h at 22 °C. The methanol was then removed under high vacuum for 48 h at 22 °C and then 5 h at 50 °C, yielding a viscous, colorless liquid.

^{1}H NMR (500 MHz, D_2O) δ (hept, $J = 6.1$ Hz, 1H), 2.89 – 2.24 (m, 12H), 1.11 (m, 3H). ^{13}C NMR (126 MHz, D_2O) δ 66.2, 65.7, 65.5, 65.3, 64.9, 62.8, 62.6, 62.1, 61.6, 56.2, 55.7, 53.7, 53.1, 51.9, 51.5, 51.1, 50.8, 50.7, 48.8, 47.7, 45.6, 39.9, 39.8, 37.8, 20.3, 19.7.

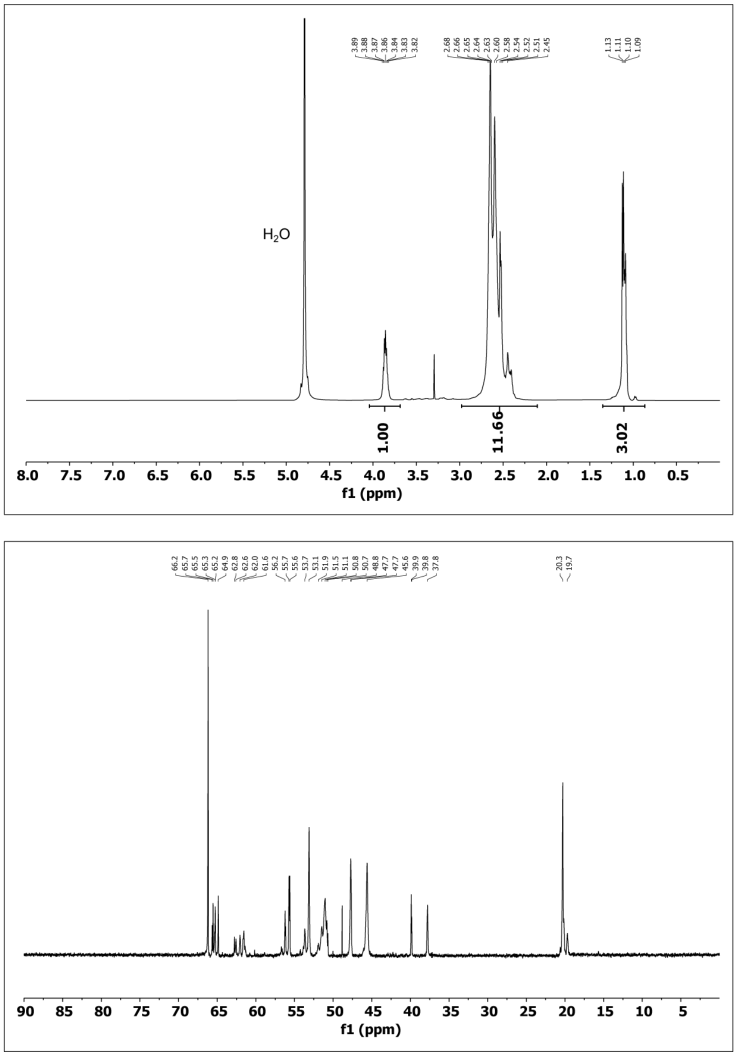

Figure S8: ^{1}H NMR spectrum (Top, 500 MHz) and ^{13}C NMR spectrum (Bottom, 126 MHz) of 0.4 O:N PO−BPEI collected in D_2O.

2.2 Differential Scanning Calorimetry (DSC)

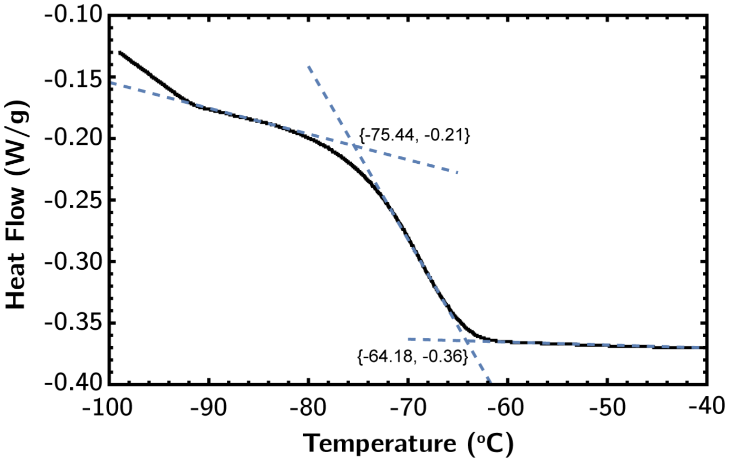

Figure S9: DSC of BPEI (MW = 800 g/mol), showing estimation of T_{ons} and T_{end} values used to determine T_g (via half-width).

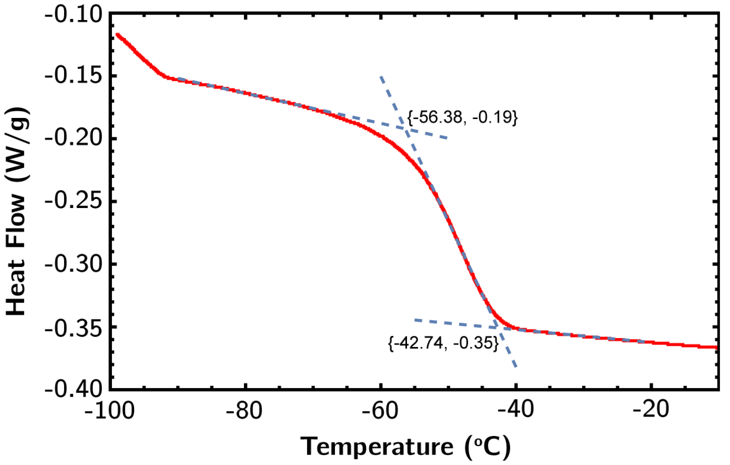

Figure S10: DSC of 0.2 O:N PO−BPEI, showing estimation of T_{ons} and T_{end} values used to determine T_g (via half-width).

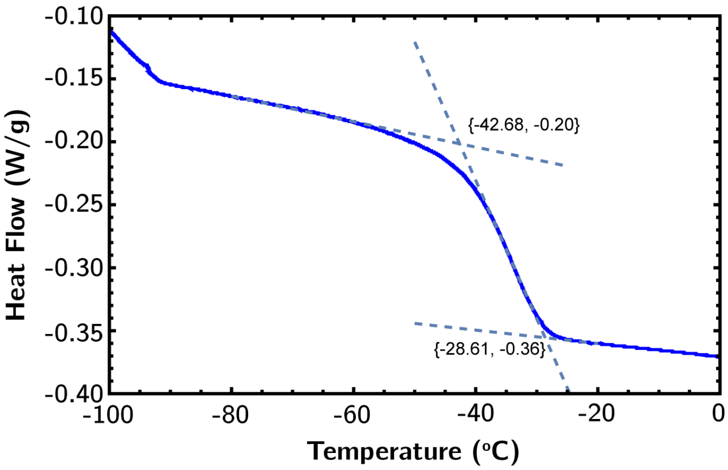

Figure S11: DSC of 0.4 O:N PO−BPEI, showing estimation of T_{ons} and T_{end} values used to determine T_g (via half-width).

2.3 Photoluminescence (PL) spectroscopy

PL experiments were performed on a custom built Princeton Instruments spectrometer using a liquid N_2-cooled Si CCD (PyLoN) array for collecting visible-NIR spectra (400-900 nm). Intensity calibration was preformed daily using an IntelliCal USB-LSVN (9000-410) calibration lamp. Samples were placed in a 2 mm quartz cuvette and excited with a 365 nm LED (7.5 nm FWHM). A 400 nm longpass filter was employed between the sample and collection fiber. Emission spectra were collected from 200-800 nm using a 150 g/mm grating with 800 nm blaze and 3 mm slit; 20 spectra were averaged with an overall exposure time of 5 seconds. Temperature control was achieved with an Oxford Instruments OptistatDN sample-in-N_2-vapor cryostat. Polymer samples were both cooled and heated at a rate of 1°C/min. The standard error was calculated by dividing the standard deviation by the square root of the sample size, typically attained from three different independent samples.

Tetrakis(4-hydroxyphenyl)ethylene (THPE) was employed as the fluorescent probe molecule in this work. The shape of the emission spectra from this probe is highly influenced by the viscosity of the matrix in which it is suspended. Details of the photophysical mechanisms responsible for this behavior are described elsewhere.[18,19] Briefly, the probe is non-emissive when well solvated in low viscosity solvents, where free rotation of the phenyl groups in the excited state provides numerous non-radiative pathways for decay back to the ground state. However, when the probe is aggregated or in a glassy matrix, restriction of these rotations to varying degrees leads to wavelength dependent emission from the excited state of the probe molecule. In this work, 0.5 wt.% THPE was stirred into each bulk polymer under N_2 in the dark at 80 °C for 1 h to ensure full dissolution of the probe. The samples were cooled at 1 °C/min to -110 °C, at which point the light source was attenuated to achieve maximum signal to noise in the emission spectrum. The samples were then heated at the same rate in order to minimize hysteresis effects, and spectra were recorded every 10 °C.

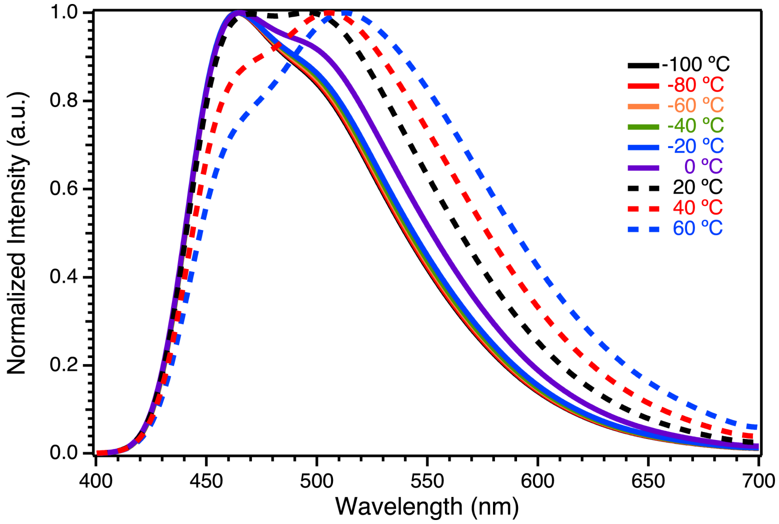

Figure S12: Normalized emission spectra of 0.5 wt.% THPE doped into 0.4 O:N PO-BPEI as a function of temperature. Excitation at 365 nm.

2.4 NMR relaxometry

T_1 and T_2 NMR relaxometry measurements were carried out with a single-sided PM2 NMR-MOUSE (Mobile Universal Surface Explorer) from Magritek GmbH, operating at a frequency of 28.05 MHz for 1H with the static magnetic field gradient of 39.9 T/m. A vial of liquid BPEI or PO-functionalized BPEI was degassed under vacuum, sotred under argon, and placed on top of the NMR MOUSE for analysis. Signals are detected by a horizontal slice detection area of 12.5 × 12.5 mm^2 configured to the max penetration depth of 1.9 mm. For these

Table S1: Spectroscopic features and statistics extracted from NMR relaxometry measurements

Sample	T1 [ms]	error	R^2	T2 (single) [ms]	error	R^2	Bi-exponential (1)	error	Bi-exponential (2)	error	R^2
BPEI	30.1	0.5	0.994	12.392	0.04	0.991	5.445	0.119	17.139	0.19	0.998
0.2 O:N PO−BPEI	36.9	1.2	0.993	1.28	0.009	0.987	2.291	0.067	0.698	0.021	0.995
0.4 O:N PO−BPEI	64.8	2.9	0.979	0.295	0.003	0.97	0.68	0.072	0.208	0.01	0.975

measurements, a slice thickness of ~100 μm (acquisition time of 6 μs) was used to reduce the echo time and maximize the acquisition volume of signal. A radio frequency pulse length of 1.8 μs with varying amplitudes was used for the 90°C and 180°C pulses in the CPMG and T_1 saturation recovery experiments for measuring T_2 and T_1, respectively. For the CPMG experiments an echo time of 28 μs was used with 1000 echoes totaling 28 ms in acquisition time and 64 scans were acquired to improve signal to noise. For T_1 saturation recovery experiments the recovery delay was incremented exponentially with 32 steps between 0 to 800 ms max recovery time, a CPMG detection was used for detecting each T_1 recovery increment using the same echo time of 28 μs, co-adding the first 100 echoes and acquiring 16 scans to improve signal to noise.

References

(1) Kresse, G.; Furthmüller, J. Efficient Iterative Schemes for Ab Initio Total-energy Calculations using a Plane-wave Basis Set. Phys. Rev. B **1996**, 54, 11169–11186.

(2) Blöchl, P. E. Projector Augmented-wave Method. Phys. Rev. B **1994**, 50, 17953–17979.

(3) Kresse, G.; Joubert, D. From Ultrasoft Pseudopotentials to the Projector Augmented-wave Method. Phys. Rev. B **1999**, 59, 1758–1775.

(4) Perdew, J. P.; Burke, K.; Ernzerhof, M. Generalized Gradient Approximation Made Simple. Phys. Rev. Lett. **1996**, 77, 3865–3868.

(5) Grimme, S.; Antony, J.; Ehrlich, S.; Krieg, H. A consistent and accurate ab initio parametrization of density functional dispersion correction (DFT-D) for the 94 elements H-Pu. The Journal of Chemical Physics **2010**, 132, 154104.

(6) Hoover, W. G. Canonical dynamics: Equilibrium phase-space distributions. Phys. Rev. A **1985**, 31, 1695–1697.

(7) Sun, J.; Ruzsinszky, A.; Perdew, J. P. Strongly Constrained and Appropriately Normed Semilocal Density Functional. Phys. Rev. Lett. **2015**, 115, 036402.

(8) Zhang, L.; Han, J.; Wang, H.; Car, R.; E, W. Deep Potential Molecular Dynamics: A Scalable Model with the Accuracy of Quantum Mechanics. Phys. Rev. Lett. **2018**, 120, 143001.

(9) Zhang, L.; Lin, D.-Y.; Wang, H.; Car, R.; E, W. Active learning of uniformly accurate interatomic potentials for materials simulation. Phys. Rev. Mater. **2019**, 3, 023804.

(10) Troullier, N.; Martins, J. L. Efficient pseudopotentials for plane-wave calculations. Phys. Rev. B **1991**, 43, 1993–2006.

(11) Parrinello, M.; Rahman, A. Crystal Structure and Pair Potentials: A Molecular-Dynamics Study. Phys. Rev. Lett. **1980**, 45, 1196–1199.

(12) Wang, H.; Zhang, L.; Han, J.; E, W. DeePMD-kit: A deep learning package for many-body potential energy representation and molecular dynamics. Computer Physics Communications **2018**, 228, 178–184.

(13) Plimpton, S. Fast Parallel Algorithms for Short-Range Molecular Dynamics. Journal of Computational Physics **1995**, 117, 1–19.

(14) Giannozzi, P. et al. Advanced capabilities for materials modelling with Quantum ESPRESSO. Journal of Physics: Condensed Matter **2017**, 29, 465901.

(15) Starr, F. W.; Nielsen, J. K.; Stanley, H. E. Hydrogen-bond dynamics for the extended simple point-charge model of water. Phys. Rev. E **2000**, 62, 579–587.

(16) Starr, F. W.; Nielsen, J. K.; Stanley, H. E. Fast and Slow Dynamics of Hydrogen Bonds in Liquid Water. Phys. Rev. Lett. **1999**, 82, 2294–2297.

(17) Huš, M.; Urbic, T. Strength of hydrogen bonds of water depends on local environment. The Journal of Chemical Physics **2012**, 136, 144305.

(18) Barbara, P. F.; Rand, S. D.; Rentzepis, P. M. Direct measurements of tetraphenylethylene torsional motion by picosecond spectroscopy. Journal of the American Chemical Society **1981**, 103, 2156–2162.

(19) Mei, J.; Leung, N. L. C.; Kwok, R. T. K.; Lam, J. W. Y.; Tang, B. Z. Aggregation-Induced Emission: Together We Shine, United We Soar! Chemical Reviews **2015**, 115, 11718–11940.